nature physics

ARTICLES

https://doi.org/10.1038/s41567-021-01268-2

Dynamics of driven polymer transport through a nanopore

Kaikai Chen[1], Ining Jou[2], Niklas Ermann[1], Murugappan Muthukumar[2], Ulrich F. Keyser[1] and Nicholas A. W. Bell[1,3]✉

The transport of polymers across nanoscale pores underpins many biological processes, such as the ejection of bacteriophage DNA into a host cell and the transfer of genes between bacteria. The movement of polymers into and out of confinement is also the basis for a wide range of sensing technologies used for single-molecule detection and sequencing. Acquiring an accurate understanding of the translocation dynamics is an essential step in the quantitative analysis of polymer structure, including the localization of binding sites or sequences. Here we use synthetic nanopores and nanostructured DNA molecules to directly measure the velocity profile of driven polymer translocation through synthetic nanopores. Our results reveal a two-stage behaviour in which the translocation initially slows with time before accelerating close to the end of the process. We also find distinct local velocity correlations as the DNA polymer chain passes through the nanopore. Brownian dynamics simulations show that the two-stage behaviour is associated with tension propagation, with correlations arising from the random-walk conformation in which the DNA begins.

Molecular transport in confined nanoscale geometries is the basis for many emerging biotechnologies and biological processes[1–3]. Polymer translocation across a nanoscale pore has been one of the most intensively studied topics in this field. Motivated in part by the goal of DNA sequencing[4], a rich phenomenology of behaviour has been observed, requiring ideas from polymer physics, surface science and fluid mechanics[5–7]. Nanopore sensors work by measuring the modulations in ionic current as single molecules are electrophoretically driven through the pore. Ever since the first demonstration of nucleic acid detection[8], intensive efforts have focused on understanding the physics governing key experimental observables such as the translocation time (τ).

For the vast majority of experiments with synthetic nanopores, the time the polymer takes to pass through a nanopore is significantly shorter than its relaxation time. Translocation is, therefore, a non-equilibrium process described in the literature by a wide variety of physical models[5,7,9–12]. Most efforts to compare experiments and theory have focussed on the scaling of translocation time with polymer length N ($\tau \approx N^{\alpha}$). A wide range of values of α have been experimentally measured[9,13–16]. These values of α can be fitted to a variety of models with different underlying physics[7,17,18], which has resulted in ongoing debates[19] and prevented a clear picture of the physics of translocation from emerging. A more direct way to measure translocation behaviour is to study the translocation speed within single individual molecules by tagging sections of the polymer at known intervals[20–22]. However, until now, this technique has not had the resolution to test different models for the translocation process.

Here we develop a method to accurately measure the dynamics of DNA within individual translocations at multiple timepoints and with a variety of nanopore geometries, enabling a new understanding of polymer transport. By applying ideas from DNA nanotechnology, we fabricate DNA molecules with positional markers that enable us to observe dynamics at an intermediate scale between the behaviour of the whole chain and individual monomers. We observe a two-stage process where the translocation slows in time before accelerating close to the end. Our measurements agree with the predictions of tension propagation theory[12], where changes in translocation velocity are determined by dynamic changes in the number of monomers of the polymer chain under tension. We also examine the physical nature of velocity fluctuations in this strongly non-equilibrium regime and find correlations in local velocity along the chain. Coarse-grained Brownian dynamics simulations recapitulate the tension propagation dynamics and reveal that the correlated motion arises from the random starting conformations of the DNA as set by entropic forces.

Figure 1a sketches the polymer just at the initiation of translocation, indicating the entropic forces and Brownian motion of the monomers due to interactions with the surrounding solvent. The electric field in the nanopore pulls the molecule into and through the pore while straightening the polymer coil. Nanopore sensing usually measures the total translocation time τ taken by the DNA to pass through the nanopore. We compare the typical timescales of driven translocation and thermal relaxation (Fig. 1a) by compiling statistics from the literature for the average translocation times τ as a function of DNA length (Fig. 1b). The synthetic nanopores have diameters in the range of 10–40 nm and therefore DNA–pore interactions are relatively weak[23]. The resulting DNA translocation times are compared with the Zimm relaxation time τ_Z of the polymer coil $\tau_Z = \frac{0.3\eta(\sqrt{N}l_0)^3}{k_B T}$, where η is the solution viscosity, N is the number of Kuhn segments, l_0 is the Kuhn length, k_B is the Boltzmann constant and T is the temperature. For all experiments, the translocation time is observed to be significantly shorter than the polymer relaxation timescale, namely, $\tau \ll \tau_Z$. We note that experiments with single-stranded nucleic acids and protein nanopores show $\tau \gg \tau_Z$ (refs. [24,25]) due to strong interactions between the nanopore and translocating DNA and have been described by quasi-equilibrium theories where the polymer chain is relaxed at all stages of translocation[26,27].

To gain a new understanding of the non-equilibrium translocation regime, we used DNA nanotechnology to pattern molecules

[1]Cavendish Laboratory, University of Cambridge, Cambridge, UK. [2]Polymer Science and Engineering Department, University of Massachusetts, Amherst, MA, USA. [3]Present address: The Francis Crick Institute, London, UK. ✉e-mail: nicholas.bell@crick.ac.uk

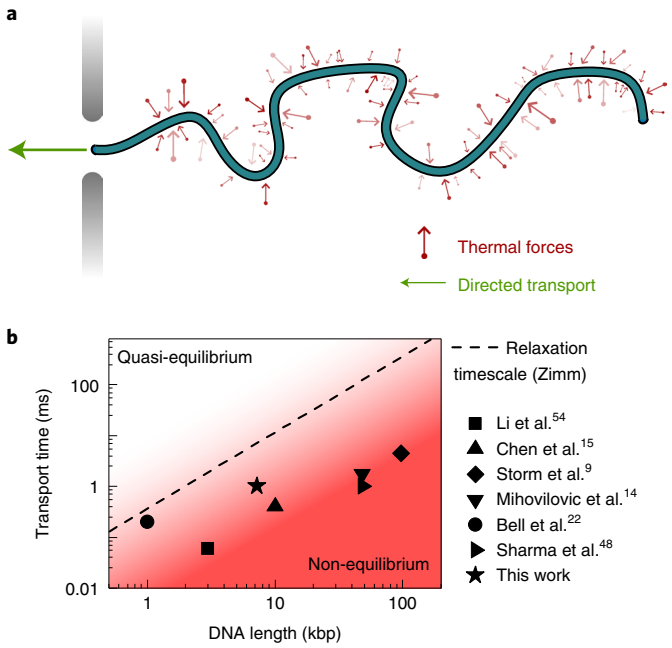

Fig. 1 | Translocation of dsDNA through synthetic nanopores is a non-equilibrium process. a, Schematic illustrating directed polymer translocation through a nanoscale aperture. The entropic forces due to thermal noise are indicated together with the driving force, for example, an electrophoretic force due to an applied potential difference. **b**, Values from the literature showing the measured translocation time of dsDNA as a function of DNA length using typical experimental conditions for measuring nanopore-based signals[14,15,48,53–55]. For the representative genomic lengths of dsDNA shown here, all translocation times measured are significantly below the Zimm time (τ_Z) and therefore in the non-equilibrium limit (see the main text for the definition of Zimm time). The Kuhn length l_0 was taken as 80 nm.

with structural motifs[20,21,28,29] and thereby enable the accurate tracking of motion within individual DNA translocations. We synthesized a double-stranded DNA (dsDNA) molecule with six markers positioned along its contour (Methods). Each marker was composed of eight DNA dumbbell hairpins that protrude from the backbone of the DNA double helix (Fig. 2a). The markers were equally spaced along the 7,228 bp contour length with a separation of 1,032 bp. We studied the translocation of this DNA construct through two types of synthetic nanopore. First, membrane-based nanopores with a diameter ranging from 13 to 17 nm were fabricated in either 20-nm-thick silicon dioxide (SiO_2) or 13-nm-thick silicon nitride (SiN_x) membranes using the dielectric breakdown method (Supplementary Figs. 1 and 2)[30] and DNA was subjected to translocation (Fig. 2b). Figure 2c shows the ionic current trace from a typical translocation through a membrane nanopore. The nanostructured DNA creates a characteristic reduction in current as it translocates through the nanopore under an applied voltage with each of the six markers creating an additional dip in the current.

The second type of synthetic nanopore used was conical glass nanopores with diameters of 14 ± 3 nm (mean ± standard deviation (s.d.)) and cone semi-angle of 0.05 ± 0.01 radians (mean ± s.d.) based on a previous characterization[29]. We consider only translocations from the open reservoir as indicated (Fig. 2d,e). There is, therefore, strong confinement in *trans* where the DNA enters after passing through the nanopore tip at which the electric field is focussed (Supplementary Fig. 3). To facilitate an unambiguous detection of the translocation end for these conical nanopores, we added an additional seventh marker at one end of the DNA construct. The voltage applied across the conical nanopore was sevenfold higher than the membrane nanopores to obtain a similar translocation speed. This is due to a lower electrophoretic force and higher friction acting on the DNA in the conical pore geometry (Supplementary Fig. 4). The DNA construct design with six markers showed a 10% reduced overall translocation time compared with DNA without markers (Supplementary Fig. 5). This small difference is likely due to the increased overall charge from the DNA dumbbell hairpins that form the markers. Each marker gave a high signal-to-noise reading, which was accurately captured at the 100 kHz measurement bandwidth of the system (Supplementary Fig. 6). For both classes of synthetic nanopores, only unfolded (single-file) translocations were selected, and a peak fitting algorithm was used to calculate the time that each marker passed through the nanopore (Supplementary Figs. 7–12)[31]. We collected statistics on thousands of translocations with multiple nanopores to enable a robust statistical analysis of the mean DNA trajectory and its variation (full details of nanopores used and statistics are given in Supplementary Section 2). Six intervals from $i=1$ to $i=6$ were defined (as shown in Fig. 2c,e) and the corresponding translocation times (τ_i) of these intervals were measured.

Figure 2f shows the histograms of the intra-event times for one example nanopore (15 nm diameter) in a 20-nm-thick SiO_2 membrane. In Fig. 2g, we plot the corresponding variation in the mean value of τ_i normalized by the first value τ_1. Figure 2h shows similar data from a conical nanopore and further experimental repeats are shown in the Supplementary Information. We consistently observe—for different nanopores and nanopore types at various voltages (seven membrane nanopores and nine conical nanopores; Supplementary Figs. 13–22)—that τ_i increases over the majority of translocation from the interval $i=1$ to $i=4$ before a substantial reduction for $i=6$. Although there is some debate about the importance of the *trans*-side friction on translocation dynamics[32–34], the fact that very similar behaviour is observed in conical glass nanopores as well as membrane pores indicates that the *trans* reservoir does not play an important role in the qualitative description of translocation dynamics. The slightly lower increase of ~5% from τ_1 to τ_4 for the conical nanopores compared with ~10% for the membrane nanopores could be explained by this difference in *trans* confinement, but it may also reflect differences in hydrodynamic friction inside the pore for the different pore types[35]. Experiments using a 14.5-kbp-long DNA molecule with 12 markers also showed a clear two-stage behaviour with slowing down over the majority of translocation followed by a speed up close to the end (Supplementary Fig. 23).

Having analysed the mean trajectories of DNA translocation, we studied the nature of fluctuations in velocity. We calculated the Pearson correlation coefficient given by $\rho\left(\tau_i, \tau_j\right) = \mathrm{cov}\left(\tau_i, \tau_j\right)/\sigma_{\tau_i}\sigma_{\tau_j}$ for different intervals along the DNA, where σ is the standard deviation, and i and j denote the interval numbers ($j = 2, 3, 4, 5; 0 < i < j$). Figure 3a shows the scatter plots of τ_2 versus τ_1 and τ_5 versus τ_1 for translocations through a 15-nm-diameter SiO_2 membrane nanopore. In Fig. 3b, we plot the variation in correlation coefficient as a function of the separation between the two intervals ($j-i$). Data for a conical glass nanopore are shown in Fig. 3c. For both types of nanopore, we observe an increasing correlation coefficient as the spacing between the two considered segments is reduced. This behaviour was consistently observed for different nanopores and at a range of voltages (Supplementary Figs. 24–27). In Fig. 3d, we plot data points from six membrane nanopores quantifying how the variance in translocation times increases as the translocation progresses. A least-squares fit to the variance scaling yielded a power law of 1.77. Experiments with conical pores yielded a scaling of 1.53 (Supplementary Fig. 28). A variety of polymer simulation models have discussed the scaling values of variance in the context of tension propagation and other translocation models[5,36–38]. However given the difficulty in comparing

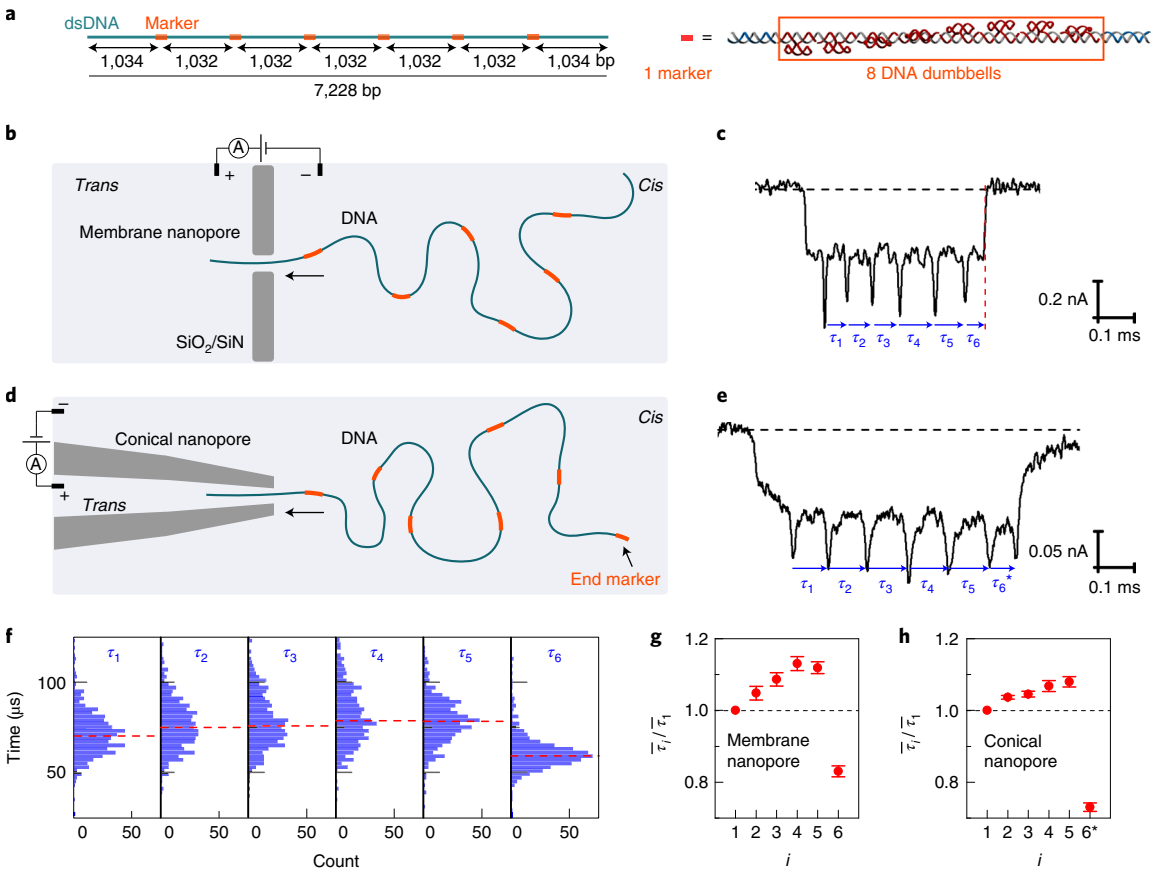

Fig. 2 | Schematic and examples of the measurement of DNA translocation velocity through synthetic nanopores. a, Outline of the DNA construct showing positions of markers along the backbone and 3D structure of each marker. Each marker comprises eight DNA dumbbells along the dsDNA strand. **b**, Schematic of DNA translocation through a membrane nanopore driven by an applied electric field. **c**, Example ionic current recording showing a single translocation through a membrane nanopore at 100 mV applied potential, with spikes showing the positional markers. **d**, Schematic of translocation through a conically shaped nanopore formed by glass capillary pulling. **e**, Example translocation through a conical nanopore at 700 mV applied potential. **f**, Histograms of τ_1 to τ_6 for a 15-nm-diameter nanopore in a SiO_2 membrane at 100 mV applied potential. The total number of translocations is $N = 548$. **g**, Results of mean time (normalized to $\overline{\tau}_1$) calculated from a Gaussian fit to the histograms in **f**. Error bars are the standard error of the mean. Multiple further examples are given in Supplementary Section 2. **h**, Results of mean time produced with one conical glass nanopore recorded at 700 mV. Here $i = 6$ is starred since the separation between the centres of the two markers is only 954 bp compared with 1,032 bp for all the other markers. Therefore, $i = 6^*$ corresponds to an increase in velocity of ~20% relative to $i = 1$. Results from more nanopores are shown in Supplementary Section 2.

scaling laws due to finite size and pore friction effects[18,39], it is difficult to draw clear conclusions on the applicability of these models from this scaling alone. As argued in the introduction, the intra-event timings and fluctuations give a clearer picture of the underlying physics. These scaling values do, however, give important information for experiments seeking to determine the position of objects bound to DNA, such as proteins and barcodes[20,29], since they directly quantify how positional uncertainty along the DNA strand increases as the translocation progresses.

Complementary to the experiments, we have performed coarse-grained simulations of dragging a model dsDNA chain through a nanopore with an applied electric field. In the coarse-grained model, the chain is made of 700 charged beads, each with a diameter of 2.5 nm. Each bead is subjected to constraints from bond stretching, dihedral angle and inter-segment excluded volume and electrostatic interactions, which model the behaviour of dsDNA[40,41]. The equilibrium bead-to-bead distance is 1.25 nm—the beads, thus, overlap to create a cross-section that approximates a cylinder (excluded volume interactions do not apply to consecutive beads along the chain; Supplementary Fig. 29). We modelled both cylindrical and conical pore geometries (Supplementary Fig. 30). Finite element analysis showed that the electric field rapidly decays away from the pore entrance (Supplementary Fig. 3). Therefore, in our Brownian dynamics simulations, we used a constant electric field inside the pore and zero electric field outside the pore as an appropriate approximation. The simulation model does not explicitly consider individual counterions and their hydrodynamics. A single simulation is realized by first relaxing the DNA in the absence of the nanopore (Supplementary Fig. 31). The first 80 beads are inserted into the pore and the potential is switched on (Fig. 4a). The electrophoretic force on each bead is determined from the electric field strength and the bead charge was taken as $0.8e^-$ to mimic the effective charge of the DNA (Supplementary Fig. 29). The translocation then proceeds until the end of the polymer chain has passed into the pore. The simulation is repeated 950 times, with each simulation having a different starting conformation of the DNA due to random thermal motion in the initial relaxation stage (see Supplementary Section 3 for in-depth details of simulations).

The simulated DNA chain was further divided into intervals formed by every ten beads (Fig. 4b). We calculated the translocation times of these intervals from bead 180 onwards (corresponding to 225 nm chain length). In Fig. 4c, we plot the values of the mean time interval defined as the difference between the arrival time of the first bead and last bead in a particular interval i at the

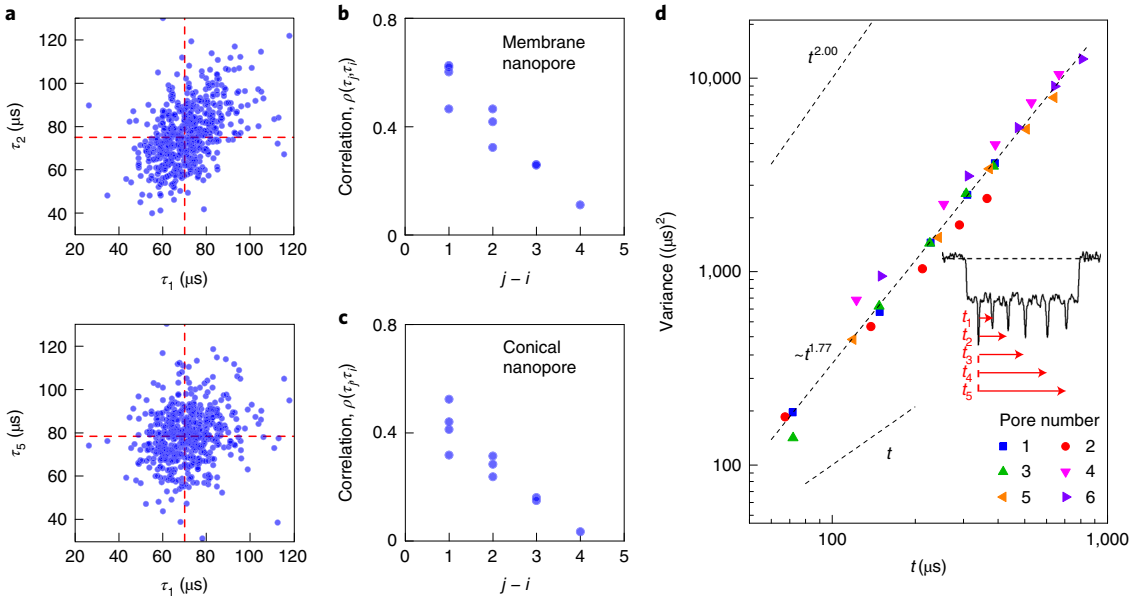

Fig. 3 | Intra-event motion correlation and cumulative spread in translocation time. a, Scatter plots comparing τ_i values (as defined in Fig. 2c) for a 15-nm-diameter SiO_2 membrane nanopore at 100 mV applied potential with a total of $N = 548$ data points. The dashed red line represents the mean value for each τ_i. **b**,**c**, Correlation coefficient as a function of separation between the two intervals considered for the membrane nanopore shown in **a** (**b**) and a conical nanopore recorded at 700 mV (**c**). $\rho(\tau_j,\tau_i)$ is the Pearson correlation coefficient of τ_j and τ_i ($j = 2, 3, 4, 5$; $0 < i < j$). **d**, Variance of translocation time distribution as a function of average translocation time using data from six membrane nanopores and five measured translocation intervals indicated in the inset. Three nanopores were measured using 60 mV and the other three using 100 mV. The fitted line has a scaling of 1.77. The slopes of quadratic and linear scaling are plotted as a guide to the eye.

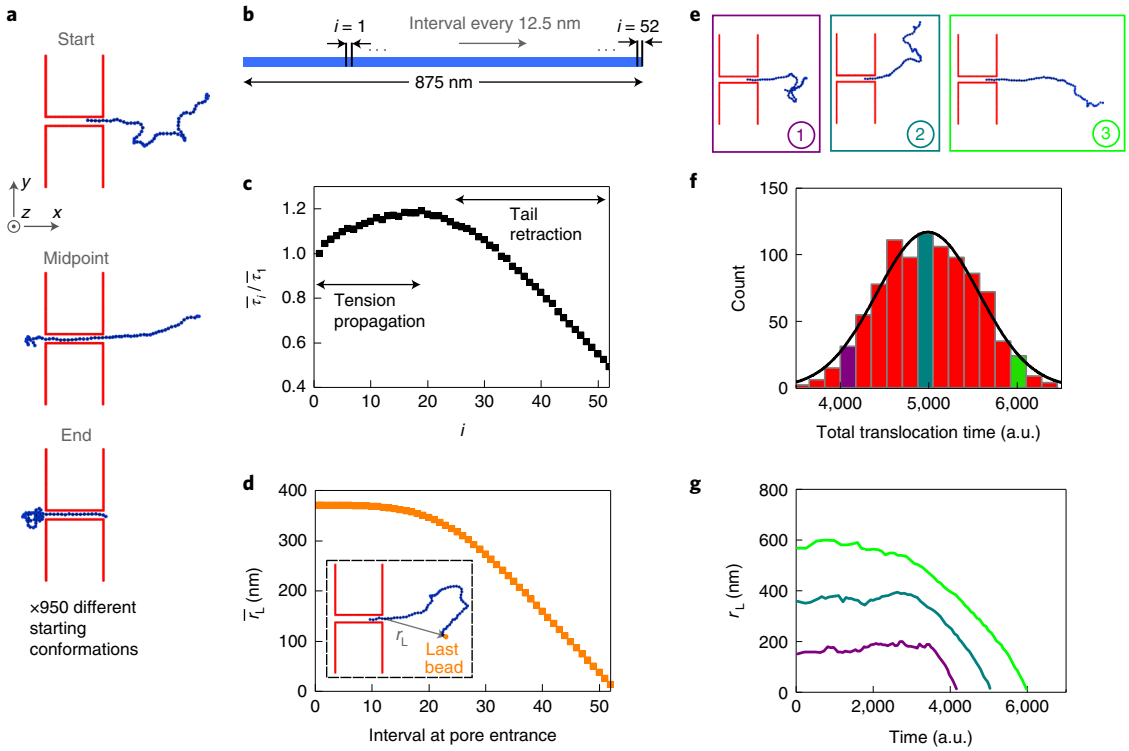

Fig. 4 | Molecular origin of two stages of DNA velocity from simulations. a, Example simulation showing the initial conformation, conformation at the midpoint when half the chain has passed through the entrance, and conformation at the end of translocation. Here 950 such simulations were performed each time using a different starting conformation of DNA. **b**, Definitions of spatial intervals along the simulated DNA. Here 52 intervals were defined, occurring every 10 beads on the 700 bead chain, starting from bead 180. The time taken for each interval τ_i (where i goes from 1 to 52) is defined as the time between the arrival of the first and last beads in that interval at the nanopore entrance. **c**, Graph showing the mean translocation time of intervals (normalized by the mean time of the first interval) calculated from all 950 simulations. **d**, Mean value of the distance of the last bead (r_L) on the chain from the pore entrance as a function of the interval that has just arrived at the pore entrance. **e**, Three examples of initial starting conformations are shown together with colours indicating their position in the distribution. **f**, Distribution of translocation times in simulations. The curve shows a Gaussian fit to the data. **g**, Position of the last bead as a function of time for the three simulations highlighted in **e**.

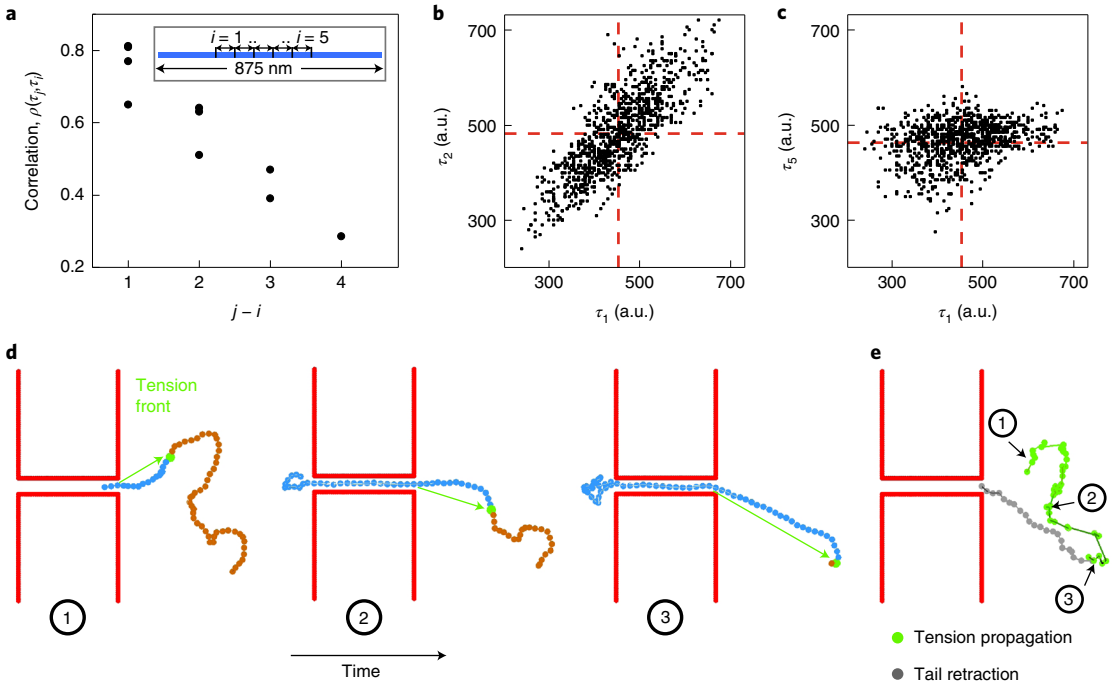

Fig. 5 | Simulations show that correlated motion arises from initial distribution of DNA conformations. a, Inset: the simulated DNA chain is divided into five intervals starting at bead 100 and ending at bead 400, with each interval being 60 beads in length. The time taken for each interval τ_i (where i goes from 1 to 5) is defined as the time between the arrival of the first and last beads in that interval at the nanopore mouth. Pearson correlation coefficient is calculated from all 950 simulations, similar to Fig. 3b,c. **b**,**c**, Scatter plots comparing τ_2 versus τ_1 (**b**) and τ_5 versus τ_1 (**c**). The red lines show the mean value for each distribution of τ_i. Time is given in simulation units. **d**, Three snapshots (time increasing from left to right) of a simulation with the position of the tension front indicated by the bead in green. The chain is coloured blue for the section that has already been pulled taut and orange for the remainder of the chain. Loops in the DNA structure are successively straightened during the translocation as the tension front follows a random path set by the initial conformation of the DNA. **e**, Overall path of tension front for the translocation illustrated in **d**, with the green line showing the path traced out during the tension propagation phase and the grey line showing the path of the last bead once the tension reaches the end of the molecule. The numbers highlight the position of the tension front at the three snapshots shown in **d**.

nanopore opening. Figure 4c reveals a two-stage process in which the translocation slows initially before speeding up. A two-stage behaviour has been predicted by tension propagation models[12,18,42] and can be related to force balance calculated for the part of the polymer chain in the *cis* reservoir that is dragged during translocation[18,43]: $F_{el} = \gamma(t)\, v(t)$, where F_{el} is the electrophoretic force acting on the DNA due to the electric field, and $\gamma(t)$ and $v(t)$ are the friction coefficient and velocity of the dragged section of the chain under tension, respectively. As the translocation progresses, successive folds of the polymer are straightened and an increasing length of the polymer chain is pulled taut and set in motion so that $\gamma(t)$ increases in time and therefore $v(t)$ decreases since F_{el} is constant. Once the tension propagates to the end of the molecule, $\gamma(t)$ decreases as the remaining tail is retracted into the nanopore, causing $v(t)$ to increase. Simulations with a conical geometry mimicking the experimental setup described in Fig. 2d showed a similar two-stage behaviour (Supplementary Fig. 32), which was observed at several different applied voltages (Supplementary Fig. 33).

In Fig. 4d, we plot the distance of the last marker on the chain from the nanopore opening (averaged over all the simulations) as a function of which interval is at the pore entrance. The last bead remains approximately at a constant position until the transition point when the translocation starts to accelerate, thereby confirming that the two-phase behaviour in translocation velocity is associated with the point at which tension has propagated through the molecule and the tail begins to retract. We note that the transition point during the two-stage behaviour occurs earlier in simulations (Fig. 4c) compared with experiments (Fig. 2g,h). The exact position of the transition is sensitive to several factors such as the DNA length and bending rigidity—longer lengths and lower bending rigidity yield a longer tension propagation phase as a fraction of the total translocation[44,45]. To enable a reasonable computation time, the simulations use a shorter length of DNA (875 nm) compared with the ~2,500 nm used for experiments, thereby creating a relatively shorter tension propagation phase[44]. However, the qualitative behaviour shows excellent agreement between simulations and experiments and reveals a clear physical picture of the two phases of translocation.

The distribution of translocation times was calculated from the simulations and is shown in Fig. 4f together with three examples of initial starting conformations (Fig. 4e). In the non-equilibrium limit, the distribution of total translocation times is mainly determined by the ensemble of initial configurations of the DNA at the start of translocation rather than Brownian fluctuations[37,43,46]. In common with previous simulations[43], we find that the total translocation time is strongly dependent on the initial starting configuration, with more stretched-out conformations resulting in higher viscous drag and hence longer translocation times as per $F_{el} = \gamma(t)\, v(t)$. The importance of the initial conformation has also been established by experiments, which showed that nanoscale confinement close to the pore entrance results in a reduction in the distribution of translocation times[47]. In Fig. 4g, we plot the distance of the last bead from the pore mouth as a function of time for the three individual translocations highlighted in Fig. 4e. For the less stretched-out conformations, as exemplified by the purple data trace, the tension propagation phase occupies a higher fraction of

the total translocation since the numerous folds must be straightened before the tension reaches the end of the molecule.

We also used our simulations to investigate the origin of the correlation in velocity between local segments of the DNA (Fig. 3b,c). The DNA chain was divided into five equally spaced intervals each corresponding to 60 beads in length. The correlation coefficient was computed for all the possible combinations of these five intervals, as shown in Fig. 5a, with example scatter plots shown in Fig. 5b,c. Figure 5b shows strongly correlated motion for the adjacent intervals τ_1 and τ_2. In good agreement with experiments, we find that the correlation coefficient decreases with increasing separation between the intervals considered (Fig. 5a).

To relate the changes in translocation velocity to the DNA conformation, we calculated the approximate position along the chain that represents the boundary between the section of the chain that has been pulled taut and set in motion towards the pore and the section that has yet to feel the tensile force (Supplementary Fig. 34 and Supplementary Video 1). In Fig. 5d, we show an example simulation with the position of this tension front highlighted in green for three selected timepoints. During the tension propagation phase, the tension front path approximately follows the course of the random walk set out by the initial DNA conformation. Once the tension front reaches the end of the molecule, the tail is then linearly retracted into the pore. Figure 5e shows the path of the tension front during translocation with the tension propagation phase shown in green and the tail retraction phase shown in grey.

The decaying velocity correlation during tension propagation is readily explained in the context of the time-varying viscous drag acting on the section of the chain that is under tension and moving towards the nanopore. At short timescales, the position of the tension front, and hence $\gamma(t)$, does not change significantly and the translocation intervals are strongly correlated. However, for two intervals separated by a long distance along the chain relative to the persistence length, the memory of the tension front position is lost due to the random walk of the initial polymer chain configuration.

In summary, we have used nanostructured DNA molecules to study the velocity profile of polymer translocation through synthetic nanopores. We experimentally find that the average translocation velocity initially decreases before an acceleration close to the end. This two-stage behaviour provides the first direct observation of tension propagation[7,12]—a non-equilibrium description of the local process of polymer straightening and unfolding during translocation. In the initial slowing phase, the tension is only felt by a local section of the polymer and the tension front propagates out towards the end of the polymer as successive folds are straightened. In the second speeding-up phase, the tension has fully propagated through the polymer and the length of tensed polymer progressively decreases as it is sucked through the pore. We also observed, in our experiments and simulations, that the translocation velocity displays correlations for local segments due to the path taken by the tension propagation front as it follows the random walk of DNA conformation. The direct measurement of polymer tension dynamics provides a framework for the exploration of advanced polymer translocation problems such as time-varying driving force, complex nanoscale pore geometries, and influence of polymer knots and folds[17,48–50]. Our new insights into the trajectory and fluctuations of DNA translocation through synthetic nanopore sensors will also impact emerging applications such as sequencing[46], DNA data storage[51] and DNA mapping[52].

Online content

Any methods, additional references, Nature Research reporting summaries, source data, extended data, supplementary information, acknowledgements, peer review information; details of author contributions and competing interests; and statements of data and code availability are available at https://doi.org/10.1038/s41567-021-01268-2.

Received: 4 March 2020; Accepted: 17 May 2021;
Published online: 24 June 2021

References

1. Pennisi, E. Search for pore-fection. *Science* **336**, 534–537 (2012).
2. Restrepo-Pérez, L., Joo, C. & Dekker, C. Paving the way to single-molecule protein sequencing. *Nat. Nanotechnol.* **13**, 786–796 (2018).
3. Marbach, S., Dean, D. S. & Bocquet, L. Transport and dispersion across wiggling nanopores. *Nat. Phys.* **14**, 1108–1113 (2018).
4. Branton, D. et al. The potential and challenges of nanopore sequencing. *Nat. Biotechnol.* **26**, 1146–1153 (2008).
5. Muthukumar, M. *Polymer Translocation* (CRC Press, 2009).
6. Ghosal, S., Sherwood, J. D. & Chang, H. C. Solid-state nanopore hydrodynamics and transport. *Biomicrofluidics* **13**, 011301 (2019).
7. Palyulin, V. V., Ala-Nissila, T. & Metzler, R. Polymer translocation: the first two decades and the recent diversification. *Soft Matter* **10**, 9016–9037 (2014).
8. Kasianowicz, J. J., Brandin, E., Branton, D. & Deamer, D. W. Characterization of individual polynucleotide molecules using a membrane channel. *Proc. Natl Acad. Sci. USA* **93**, 13770–13773 (1996).
9. Storm, A. J. et al. Fast DNA translocation through a solid-state nanopore. *Nano Lett.* **5**, 1193–1197 (2005).
10. Ghosal, S. Effect of salt concentration on the electrophoretic speed of a polyelectrolyte through a nanopore. *Phys. Rev. Lett.* **98**, 238104 (2007).
11. Grosberg, A. Y., Nechaev, S., Tamm, M. & Vasilyev, O. How long does it take to pull an ideal polymer into a small hole? *Phys. Rev. Lett.* **96**, 228105 (2006).
12. Sakaue, T. Nonequilibrium dynamics of polymer translocation and straightening. *Phys. Rev. E* **76**, 021803 (2007).
13. Li, J. & Talaga, D. S. The distribution of DNA translocation times in solid-state nanopores. *J. Phys. Condens. Matter* **22**, 454129 (2010).
14. Mihovilovic, M., Hagerty, N. & Stein, D. Statistics of DNA capture by a solid-state nanopore. *Phys. Rev. Lett.* **110**, 028102 (2013).
15. Chen, P. et al. Probing single DNA molecule transport using fabricated nanopores. *Nano Lett.* **4**, 2293–2298 (2004).
16. Carson, S., Wilson, J., Aksimentiev, A. & Wanunu, M. Smooth DNA transport through a narrowed pore geometry. *Biophys. J.* **107**, 2381–2393 (2014).
17. Panja, D., Barkema, G. T. & Kolomeisky, A. B. Through the eye of the needle: recent advances in understanding biopolymer translocation. *J. Phys. Condens. Matter* **25**, 413101 (2013).
18. Ikonen, T., Bhattacharya, A., Ala-Nissila, T. & Sung, W. Unifying model of driven polymer translocation. *Phys. Rev. E* **85**, 051803 (2012).
19. Wanunu, M. Nanopores: a journey towards DNA sequencing. *Phys. Life Rev.* **9**, 125–158 (2012).
20. Singer, A., Rapireddy, S., Ly, D. H. & Meller, A. Electronic barcoding of a viral gene at the single-molecule level. *Nano Lett.* **12**, 1722–1728 (2012).
21. Plesa, C. et al. Velocity of DNA during translocation through a solid-state nanopore. *Nano Lett.* **15**, 732–737 (2015).
22. Bell, N. A. W. & Keyser, U. F. Specific protein detection using designed DNA carriers and nanopores. *J. Am. Chem. Soc.* **137**, 2035–2041 (2015).
23. Wanunu, M., Sutin, J., McNally, B., Chow, A. & Meller, A. DNA translocation governed by interactions with solid-state nanopores. *Biophys. J.* **95**, 4716–4725 (2008).
24. Katkar, H. H. & Muthukumar, M. Role of non-equilibrium conformations on driven polymer translocation. *J. Chem. Phys.* **148**, 024903 (2018).
25. Meller, A., Nivon, L. & Branton, D. Voltage-driven DNA translocations through a nanopore. *Phys. Rev. Lett.* **86**, 3435–3438 (2001).
26. Muthukumar, M. Polymer translocation through a hole. *J. Chem. Phys.* **111**, 10371–10374 (1999).
27. Sung, W. & Park, P. J. Polymer translocation through a pore in a membrane. *Phys. Rev. Lett.* **77**, 783–786 (1996).
28. Rothemund, P. W. K. Folding DNA to create nanoscale shapes and patterns. *Nature* **440**, 297–302 (2006).
29. Bell, N. A. W. & Keyser, U. F. Digitally encoded DNA nanostructures for multiplexed, single-molecule protein sensing with nanopores. *Nat. Nanotechnol.* **11**, 645–651 (2016).
30. Kwok, H., Briggs, K. & Tabard-Cossa, V. Nanopore fabrication by controlled dielectric breakdown. *PLoS ONE* **9**, e92880 (2014).
31. Chen, K. et al. Ionic current-based mapping of short sequence motifs in single DNA molecules using solid-state nanopores. *Nano Lett.* **17**, 5199–5205 (2017).
32. Saito, T. & Sakaue, T. *Cis–trans* dynamical asymmetry in driven polymer translocation. *Phys. Rev. E* **88**, 042606 (2013).
33. Dubbeldam, J. L. A., Rostiashvili, V. G. & Vilgis, T. A. Driven translocation of a polymer: role of pore friction and crowding. *J. Chem. Phys.* **141**, 124112 (2014).
34. Sarabadani, J. et al. Driven translocation of a semi-flexible polymer through a nanopore. *Sci. Rep.* **7**, 7423 (2017).
35. Ghosal, S. Electrophoresis of a polyelectrolyte through a nanopore. *Phys. Rev. E* **74**, 041901 (2006).
36. Dubbeldam, J. L. A., Rostiashvili, V. G., Milchev, A. & Vilgis, T. A. Driven translocation of a polymer: fluctuations at work. *Phys. Rev. E* **87**, 032147 (2013).

37. de Haan, H. W., Sean, D. & Slater, G. W. Reducing the variance in the translocation times by prestretching the polymer. *Phys. Rev. E* **98**, 022501 (2018).
38. Sarabadani, J., Ikonen, T. & Ala-Nissila, T. Iso-flux tension propagation theory of driven polymer translocation: the role of initial configurations. *J. Chem. Phys.* **141**, 214907 (2014).
39. Saito, T. & Sakaue, T. Dynamical diagram and scaling in polymer driven translocation. *Eur. Phys. J. E* **34**, 135 (2011).
40. Forrey, C. & Muthukumar, M. Langevin dynamics simulations of genome packing in bacteriophage. *Biophys. J.* **91**, 25–41 (2006).
41. Forrey, C. & Muthukumar, M. Langevin dynamics simulations of ds-DNA translocation through synthetic nanopores. *J. Chem. Phys.* **127**, 015102 (2007).
42. Sarabadani, J. & Ala-Nissila, T. Theory of pore-driven and end-pulled polymer translocation dynamics through a nanopore: an overview. *J. Phys. Condens. Matter* **30**, 274002 (2018).
43. Lu, B., Albertorio, F., Hoogerheide, D. P. & Golovchenko, J. A. Origins and consequences of velocity fluctuations during DNA passage through a nanopore. *Biophys. J.* **101**, 70–79 (2011).
44. Adhikari, R. & Bhattacharya, A. Driven translocation of a semi-flexible chain through a nanopore: a Brownian dynamics simulation study in two dimensions. *J. Chem. Phys.* **138**, 204909 (2013).
45. Ikonen, T., Bhattacharya, A., Ala-Nissila, T. & Sung, W. Influence of non-universal effects on dynamical scaling in driven polymer translocation. *J. Chem. Phys.* **137**, 085101 (2012).
46. Saito, T. & Sakaue, T. Process time distribution of driven polymer transport. *Phys. Rev. E* **85**, 061803 (2012).
47. Briggs, K. et al. DNA translocations through nanopores under nanoscale preconfinement. *Nano Lett.* **18**, 660–668 (2018).
48. Kumar Sharma, R., Agrawal, I., Dai, L., Doyle, P. S. & Garaj, S. Complex DNA knots detected with a nanopore sensor. *Nat. Commun.* **10**, 4473 (2019).
49. Mondal, D. & Muthukumar, M. Stochastic resonance during a polymer translocation process. *J. Chem. Phys.* **144**, 144901 (2016).
50. Sarabadani, J., Ikonen, T. & Ala-Nissila, T. Theory of polymer translocation through a flickering nanopore under an alternating driving force. *J. Chem. Phys.* **143**, 074905 (2015).
51. Chen, K. et al. Digital data storage using DNA nanostructures and solid-state nanopores. *Nano Lett.* **19**, 1210–1215 (2019).
52. Venkatesan, B. M. & Bashir, R. Nanopore sensors for nucleic acid analysis. *Nat. Nanotechnol.* **6**, 615–624 (2011).
53. Bell, N. A. W., Muthukumar, M. & Keyser, U. F. Translocation frequency of double-stranded DNA through a solid-state nanopore. *Phys. Rev. E* **93**, 022401 (2016).
54. Li, J., Gershow, M., Stein, D., Brandin, E. & Golovchenko, J. A. DNA molecules and configurations in a solid-state nanopore microscope. *Nat. Mater.* **2**, 611–615 (2003).
55. Storm, A., Chen, J., Zandbergen, H. & Dekker, C. Translocation of double-strand DNA through a silicon oxide nanopore. *Phys. Rev. E* **71**, 051903 (2005).

Methods

Fabrication of nanopores. Twenty-nanometre-thick SiO_2 membrane chips ($15\times15\,\mu m$ window) were purchased from Nanopore Solutions (Portugal) and 13 ± 1 nm thick SiN_x membrane chips (NT001Z-Hi-Res; $10\times10\,\mu m$ window) from Norcada (Canada). Nanopores were fabricated using the controlled dielectric breakdown method[30] with final diameters between 10 and 20 nm. The SiO_2 and SiN_x chips were mounted into polydimethylsiloxane flow cells and then filled with 1 M KCl, 10 mM Tris-HCl (pH 10.0) and 1 mM EDTA. A 10 V voltage was applied to form a <10 nm nanopore and then the pore was enlarged to the desired size by applying voltage pulses (see Supplementary Section 1 for further details). Then, the flow cell was filled with 3 M LiCl, 10 mM Tris-HCl (pH 9.0) and 1 mM EDTA for DNA translocation measurements. The conical glass nanopores were fabricated by pulling quartz glass capillaries using a P-2000 laser-heated puller (Sutter Instruments). The glass capillaries were then sealed in a polydimethylsiloxane flow cell and filled with 3 M LiCl, 10 mM Tris-HCl (pH 9.0) and 1 mM EDTA.

Synthesis of DNA. The DNA was made by annealing linearized M13mp18 single-stranded DNA together with complementary oligonucleotides to form the desired structure. Sequence details of all the strands and synthesis protocols are given in Supplementary Section 4.

Nanopore measurement. The DNA sample was diluted to a final concentration of 0.5–1.0 nM and then added into the *cis* side of the flow cell. All the results shown in the manuscript were measured in 3 M LiCl, 10 mM Tris buffer (pH 9.0) and 1 mM EDTA. Further results using 4 M LiCl with glass nanopores are shown in Supplementary Section 3. A positive voltage (60 or 100 mV for membrane nanopores and 700 mV for conical glass nanopores) was applied on the *trans* side to drive the DNA through the nanopore. The ionic current signals were recorded with an Axopatch 200B amplifier (Molecular Devices) and then filtered with an external filter (model 3382, Krohn-Hite) at 200 kHz together with the 100 kHz internal filter of the Axopatch amplifier. The current trace was recorded via a data acquisition card (PCI-6251, National Instruments) at a sampling frequency of 1 MHz. Custom-made LabVIEW 2013 (National Instruments) programs were used to remove fragments of the full-length DNA from the analysis and select only unfolded DNA translocations[29].

Simulations. Langevin dynamics simulations of dsDNA undergoing translocation through the nanopore in the presence of an applied electric field were performed using the large-scale atomic/molecular massively parallel simulator following our earlier protocol[40,41]. Full details are given in Supplementary Section 3. Supplementary Video 1 shows 15 example simulations for translocations through a membrane geometry nanopore with the position of the tension front highlighted in green. The two frames show orthogonal viewpoints of the three-dimensional (3D) simulation.

Reporting Summary. Further information on research design is available in the Nature Research Reporting Summary linked to this article.

Data availability

Source data are provided with this paper. Raw data of ionic current values for translocations together with a table summarizing all the nanopores used are available at https://doi.org/10.17863/CAM.69631.

Code availability

The code used for data collection and analysis and the code used for simulation analysis are available upon request from the corresponding author.

Acknowledgements

This work was supported by an ERC consolidator grant (no. 647144) for N.A.W.B., K.C. and U.F.K. and a National Institute of Health grant (no. 5R01HG002776-15) for I.J. and M.M. N.E. acknowledges funding from the EPSRC; Cambridge Trust; and Trinity Hall, Cambridge.

Author contributions

N.A.W.B., K.C. and U.F.K. designed the experiments. K.C., N.E. and N.A.W.B. performed the experiments. M.M. and I.J. performed the simulations. M.M., I.J. and N.A.W.B. analysed the simulation results. The paper was written through contributions of all the authors.

Competing interests

The authors declare no competing interests.

Additional information

Supplementary information The online version contains supplementary material available at https://doi.org/10.1038/s41567-021-01268-2.

Correspondence and requests for materials should be addressed to N.A.W.B.

Peer review information *Nature Physics* thanks Vincent Tabard-Cossa and the other, anonymous, reviewer(s) for their contribution to the peer review of this work.

Reprints and permissions information is available at www.nature.com/reprints.

nature research

Corresponding author(s): Dr Nicholas Bell

Last updated by author(s): May 10, 2021

Reporting Summary

Nature Research wishes to improve the reproducibility of the work that we publish. This form provides structure for consistency and transparency in reporting. For further information on Nature Research policies, see Authors & Referees and the Editorial Policy Checklist.

Statistics

For all statistical analyses, confirm that the following items are present in the figure legend, table legend, main text, or Methods section.

n/a	Confirmed
☐	☒ The exact sample size (*n*) for each experimental group/condition, given as a discrete number and unit of measurement
☐	☒ A statement on whether measurements were taken from distinct samples or whether the same sample was measured repeatedly
☒	☐ The statistical test(s) used AND whether they are one- or two-sided *Only common tests should be described solely by name; describe more complex techniques in the Methods section.*
☒	☐ A description of all covariates tested
☒	☐ A description of any assumptions or corrections, such as tests of normality and adjustment for multiple comparisons
☐	☒ A full description of the statistical parameters including central tendency (e.g. means) or other basic estimates (e.g. regression coefficient) AND variation (e.g. standard deviation) or associated estimates of uncertainty (e.g. confidence intervals)
☒	☐ For null hypothesis testing, the test statistic (e.g. *F*, *t*, *r*) with confidence intervals, effect sizes, degrees of freedom and *P* value noted *Give P values as exact values whenever suitable.*
☒	☐ For Bayesian analysis, information on the choice of priors and Markov chain Monte Carlo settings
☒	☐ For hierarchical and complex designs, identification of the appropriate level for tests and full reporting of outcomes
☒	☐ Estimates of effect sizes (e.g. Cohen's *d*, Pearson's *r*), indicating how they were calculated

Our web collection on statistics for biologists contains articles on many of the points above.

Software and code

Policy information about availability of computer code

Data collection	The data was collected using software written with labview 2013 (National Instruments).
Data analysis	Data analysis was also performed using software written with labview 2013 (National Instruments).

For manuscripts utilizing custom algorithms or software that are central to the research but not yet described in published literature, software must be made available to editors/reviewers. We strongly encourage code deposition in a community repository (e.g. GitHub). See the Nature Research guidelines for submitting code & software for further information.

Data

Policy information about availability of data

All manuscripts must include a data availability statement. This statement should provide the following information, where applicable:

- Accession codes, unique identifiers, or web links for publicly available datasets
- A list of figures that have associated raw data
- A description of any restrictions on data availability

Raw data of ionic current values for translocations together with a table summarizing all the nanopores used is available at https://doi.org/10.17863/CAM.69631.

Field-specific reporting

Please select the one below that is the best fit for your research. If you are not sure, read the appropriate sections before making your selection.

☒ Life sciences ☐ Behavioural & social sciences ☐ Ecological, evolutionary & environmental sciences

For a reference copy of the document with all sections, see nature.com/documents/nr-reporting-summary-flat.pdf

Life sciences study design

All studies must disclose on these points even when the disclosure is negative.

Sample size	Each nanopore device was run for as long as possible ie as many DNA translocations as possible were measured before the device failed. Typically this is due to clogging of the nanopore. Therefore there is no set sample size. However we only used devices where we measured a minimum of 100 unfolded translocations (as set out in Table S1+S2 of the SI). This limit was chosen so that the trends in DNA translocation velocity were clearly within the error bars of the measurement - see Figure S13.
Data exclusions	Our model is only appropriate for unfolded DNA translocations where the DNA moves in a head to tail fashion. In the measurements we also have folded translocations and fragments of DNA which must be excluded for accurate comparison with the model. In the SI (Figure S11+S12) we give examples of these excluded events and cite a previous paper published by the authors which determined the criteria for excluding these events.
Replication	The measurement shown in the main text was repeated using 6 different membrane nanopore devices. These results are presented in the supplementary information. Each repeat successfully confirmed the central findings namely a two stage translocation velocity behaviour and a decreasing correlation coefficient as a function of increasing chain separation.
Randomization	Randomization was not relevant to this study since we were not comparing experimental groups.
Blinding	Blinding was not relevant to this study since we were not comparing experimental groups.

Reporting for specific materials, systems and methods

We require information from authors about some types of materials, experimental systems and methods used in many studies. Here, indicate whether each material, system or method listed is relevant to your study. If you are not sure if a list item applies to your research, read the appropriate section before selecting a response.

Materials & experimental systems

n/a	Involved in the study
☒	☐ Antibodies
☒	☐ Eukaryotic cell lines
☒	☐ Palaeontology
☒	☐ Animals and other organisms
☒	☐ Human research participants
☒	☐ Clinical data

Methods

n/a	Involved in the study
☒	☐ ChIP-seq
☒	☐ Flow cytometry
☒	☐ MRI-based neuroimaging